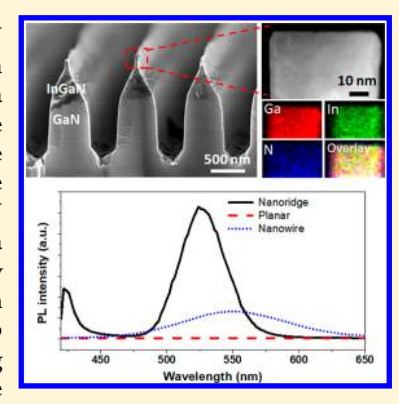


Heteroepitaxy of Fin-Shaped InGaN Nanoridge Using Molecular **Beam Epitaxy**

Yong-Bum Park,[†] Jiseok Gim,[‡] Reed Yalisove,[‡] Robert Hovden,[‡] and Zetian Mi^{*,†}

Supporting Information

ABSTRACT: We have demonstrated a well-ordered In-rich single crystalline InGaN nanoridge array grown on GaN/sapphire substrate using the integration of top-down etching and bottom-up molecular beam epitaxy. During the initial growth of InGaN on a patterned GaN/sapphire substrate, a (1011) r-plane predominantly forms, suppressing the growth in [1011] crystal direction and resulting in a triangular InGaN nanoprism. As the growth proceeds further, a narrow (~50 nm) single-crystal fin-shaped InGaN nanoridge forms atop the InGaN nanoprism structure. The resulting narrow fin-shaped InGaN nanoridge structure shows extremely strong photoluminescence (PL) intensity with a center wavelength at 524-560 nm and narrow distribution compared to the epitaxially grown planar InGaN layer or InGaN nanowire. High-resolution scanning transmission electron microscopy (STEM) combined with an energy-dispersive X-ray (EDS) map reveals that a sharply faceted single-crystal InGaN nanoridge (~50 nm width) forms along the top of each InGaN nanoprism and is composed of Ga, In, and N without phase segregation or dislocation. The single-crystalline In-rich InGaN nanoridge will pave the way to design a viable architecture for a broad range of III-nitride devices.



rowth of highly crystalline In-rich In, Ga_{1-x}N is one of I the most important technologies for III-nitride semiconductor devices. The tunability of its direct bandgap energies from ~0.65 to 3.4 eV makes it a very promising material for a broad range of optoelectronic devices including light-emitting diodes (LEDs), 1,2 lasers, solar cells, 3,4 and photoelectrochemical cells⁵⁻⁷ as well as electronic devices such as high mobility transistors. 8-10 However, creating highly crystalline In-rich In_xGa_{1-x}N heterostructures is difficult due to defects, threading dislocations, and stacking faults caused by the lattice mismatch between InN and GaN (-11%). To address these issues, nanowire, 14-18 nanoridge, and nanowall¹⁹⁻²² structures have been created that incorporate indium into GaN crystal. These nanostructures have low densities of extended defects and efficient surface stress relaxation in lattice-mismatched heterojunctions¹⁵ so they can incorporate high In content in their structures, thereby tuning the wavelength in the entire visible and near-infrared spectrum.¹⁴

Although nanowire structures have been extensively studied, there have been very few reports on the growth of InGaN nanoridge or nanowall structures. Compared to conventional nanowires, the unique structure of nanoridges or nanowalls makes them well-suited for edge-emitting lasers and fin field effect transistors.²³ As wall thickness approaches a few nanometers, In(Ga)N can exhibit unusually large exciton binding energy (up to 1.4 eV),²⁴ which rivals that of the

extensively studied single-layer transitional metal dichalcogenides and therefore offers a new quantum material platform.

To date, however, the fabrication, synthesis, and characterization of InGaN nanoridge or nanowall structures is still in its nascent stage. Recently, Chouksey et al. reported well-ordered InGaN nanowall structure, but their approach to fabrication relies solely on top-down etching of InGaN film, which is fundamentally limited by the aforementioned difficulties in planar structures showing peak emission below 500 nm wavelength.²⁵ Random InGaN nanowall networks can be formed during epitaxy of InGaN epilayers on a Si substrate, but these networks exhibit uncontrollable size, morphology, and properties.²⁰ To date, there has been no demonstration of the controlled synthesis of InGaN nanoridge or nanowall arrays using a bottom-up approach.

We have combined top-down etching and bottom-up molecular beam epitaxy to create a new method of fabricating well-ordered InGaN nanoridge arrays. We also investigated the effects of the growth conditions on the structural and optical properties of these nanoridge arrays. InGaN nanoridges are formed on a Ga-polarity c-plane. Initial growth of InGaN on a patterned GaN/sapphire substrate is limited by the dominant formation of the $(10\overline{1}1)$ plane. Increasing the growth duration

Received: August 12, 2018 Revised: September 13, 2018 Published: September 17, 2018

Department of Electrical Engineering and Computer Science, Center for Photonics and Multiscale Nanomaterials, University of Michigan, 1301 Beal Avenue, Ann Arbor, Michigan 48109-2122, United States

^{*}Department of Materials Science and Engineering, University of Michigan, 2300 Hayward Street, Ann Arbor, Michigan 48109-2117. United States

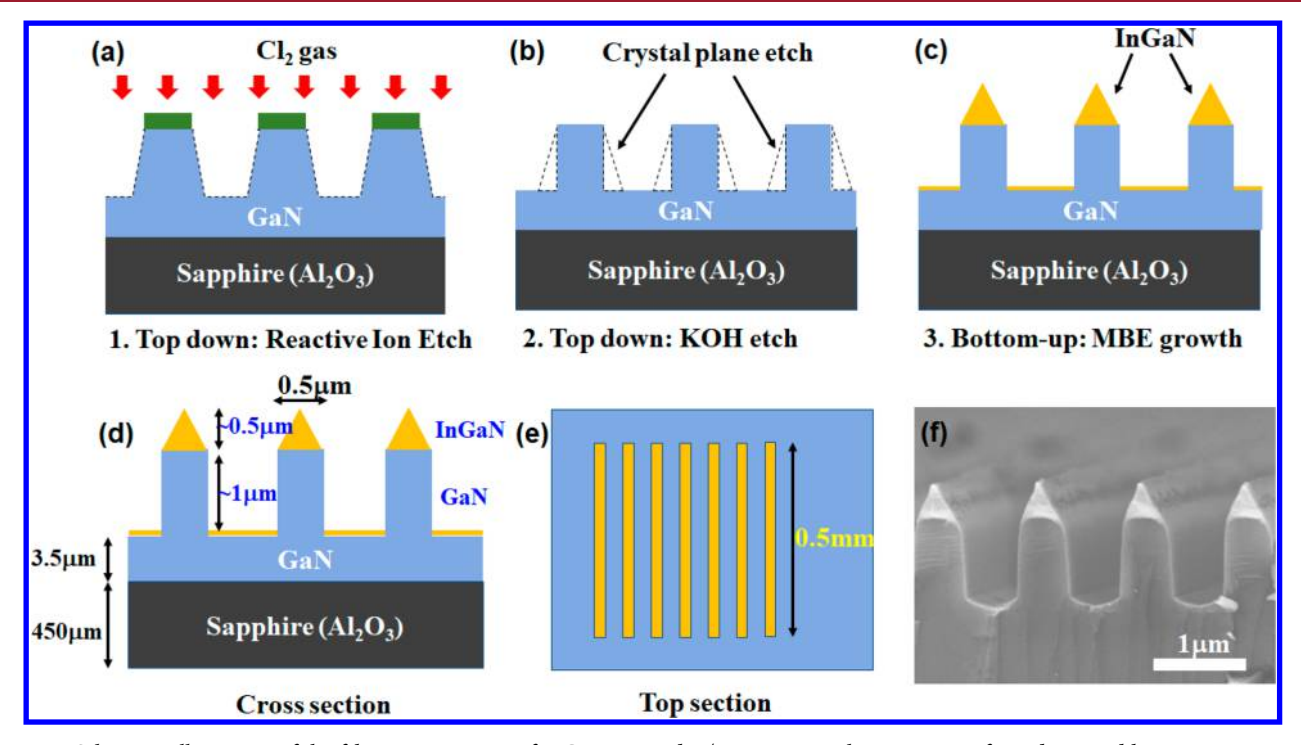


Figure 1. Schematic illustration of the fabrication process of InGaN nanoridge/nanoprism with integration of top-down and bottom-up approach. Top-down: (a) RIE etching and (b) KOH crystallographic wet etching of GaN nanowall array. Bottom-up: (c) MBE growth of InGaN on GaN nanowall array. (d) Cross-sectional view and (e) top view illustration of the nanoridge/nanoprism dimension. (f) SEM of cross-sectional InGaN nanoridge/nanoprism array.

leads to the formation of a very narrow (~50 nm) fin-shaped InGaN nanoridge structure above the InGaN nanoprism array. The resulting fin-shaped InGaN nanoridge structure shows strong photoluminescence (PL) intensity with wavelength centered at 524-560 nm and a narrow line width as compared to previously reported InGaN nanowire structure. Highresolution high-angle angular-dark-field (HAADF) suggests that the InGaN nanoridge exhibits single-crystalline structure largely free of phase separation or dislocations with homogeneous In-distribution throughout the growth direction. These improvements over previously reported nanowire $^{14-18}$ or nanoridge/nanowall structures $^{19-21}$ are attributed to the combination of the top-down and bottom-up method, which will be useful for device fabrication. This study provides not only a better understanding of InGaN epitaxial growth but also benefits the development of nanostructured InGaN-based electronic devices.

GaN nanowall structures were formed by projection lithography and etching on an n-type GaN template on a sapphire substrate. First, a stripe pattern of silicon dioxide (SiO₂) was patterned on the GaN template parallel to the [11 $\overline{20}$] a-direction. With the SiO₂ as a masking layer, 1 μ m of n-type GaN was etched by LAM 9400 inductively coupled plasma (ICP)-reactive ion etching (RIE) with Cl₂ gas as shown in Figure 1a. Transformer coupled plasma (TCP) power of 600 W and radio frequency (RF) bias of 300 W were used with flowing 30 sccm of Cl₂ gas while maintaining pressure of 2 mTorr for ICP-RIE. Please refer to Figure S1 for further details. Subsequently, the sample was immersed in 30 wt % KOH solution at elevated temperature of 120 °C for 5 min to reveal the crystal plane and to achieve smooth and vertical sidewall as shown in Figure 1b. 26,27 Finally, the SiO₂ masking layer was removed using HF solution. SEM images of the GaN nanowalls after each step are shown in Figure S1.

In this study, the GaN nanowall template had a wall width, spacing, and height of 500 nm, 400–500 nm, and 1 μm , respectively (Figure 1d). Smaller sizes can be readily achieved using e-beam lithography. The length of each segment of GaN nanowall was 0.5 mm as indicated in Figure 1e. The sample was subsequently loaded in a Veeco Gen II MBE system equipped with a radio frequency plasma-assisted nitrogen source for InGaN growth. For studying the growth conditions of the InGaN, the III–N ratio was varied by altering nitrogen flow rate from 1.5 sccm down to 0.45 sccm. In beam equivalent pressure (BEP) was maintained at 9.8 \times 10⁻⁸ Torr, Ga BEP at 2.7 \times 10⁻⁸ Torr, and growth temperature at 755 °C. Samples A–C had nitrogen flow rates of 1.5, 0.8, and 0.45 sccm, respectively, as listed in Table 1. Because of the In desorption

Table 1. MBE Growth Conditions for InGaN Nanoridge.

sample	Ga flux/Torr	In flux/Torr	N ₂ flow/sccm	III-V ratio
A	2.7e-8	9.8e-8	1.5	N ₂ -rich
В	2.7e-8	9.8e-8	0.8	N ₂ -rich
C	2.7e-8	9.8e-8	0.45	metal-rich

above 540 $^{\circ}$ C, 28 an accurate III–V ratio is difficult to determine, so the boundary between the metal- and nitrogenrich conditions was determined by the presence of metal droplets on the sample.

We investigated the effect of nitrogen flow rate on the epitaxy of InGaN nanostructures. For sample A, the abundance of nitrogen plasma induces 3-dimensional growth of the InGaN grown on the GaN nanowall template, as shown in Figure 2a and b. As the plasma flow was reduced to 0.8 sccm, we observed less roughness on the InGaN, but nanoscale roughness was still present on the surface, as illustrated in Figure 2c and d. Once the nitrogen flow reached 0.45 sccm in

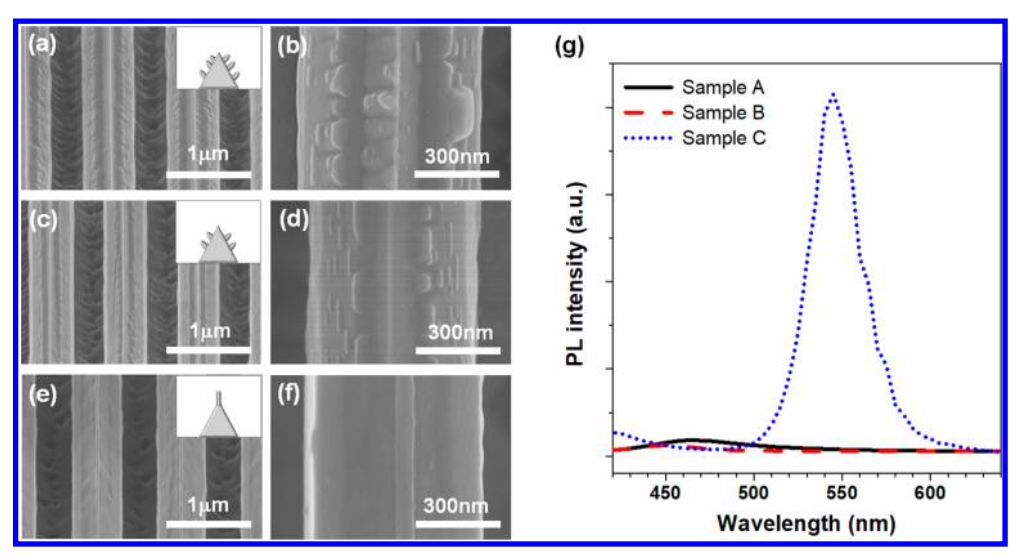


Figure 2. Bird's eye view SEM image of InGaN/GaN structure grown in MBE under the conditions of samples (a) A, (c) B, and (e) C. The inset shows the cross-sectional schematic illustration of surface roughness after growth. High-resolution top-down view of SEM image of InGaN nanostructure grown in MBE under the conditions of samples (b) A, (d) B, and (f) C. Refer to Table 1 for the growth conditions of each sample. (g) Room-temperature micro-PL emission comparison of InGaN nanostructure under sample A (black solid line), sample B (red dashed line), and sample C (blue short dotted line) conditions. The peak wavelengths are at 468, 452, and 545 nm for InGaN nanostructure with sample A, B, and C conditions, respectively.

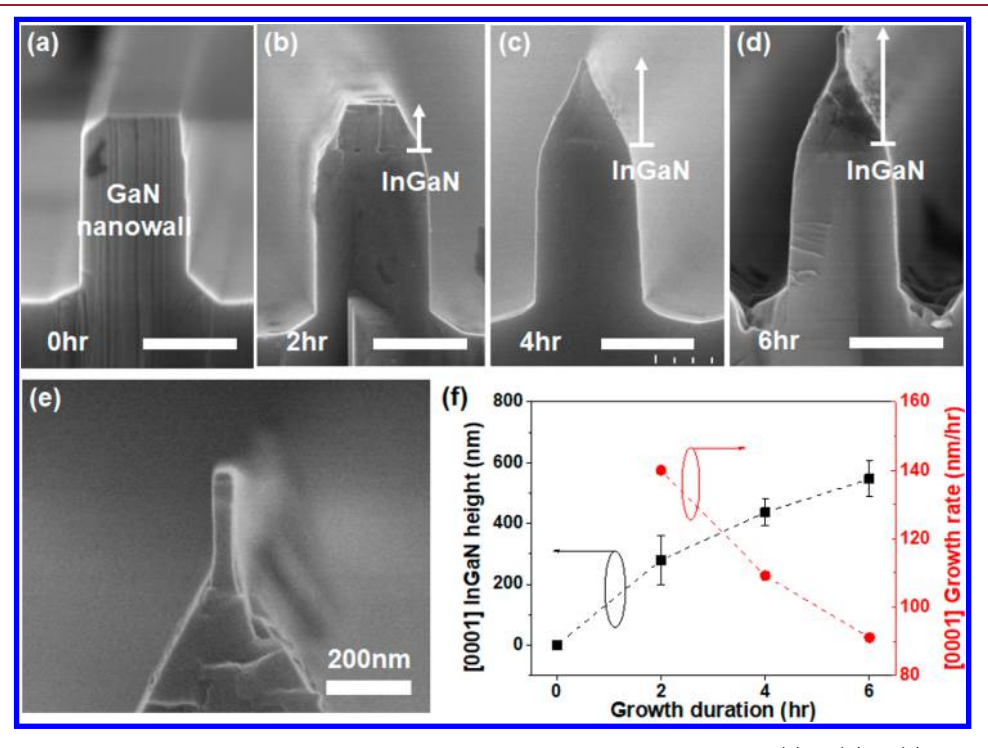


Figure 3. Cross-sectional SEM image of single GaN nanowall segment with InGaN growth duration of (a) 0, (b) 2, (c) 4, and (d) 6 h. In (b-d), the InGaN region is shown with arrows to indicate the growth length along the *c*-axis. All scale bars represent 500 nm unless specified. (e) High-magnification cross-sectional SEM image of very narrow fin-shaped InGaN nanoridge elongated on top of InGaN nanoprism after 6 h of growth. (f) Measured InGaN height (black square) and calculated [0001] direction growth rate (red circle) with respect to growth time.

sample C, the InGaN surface became smooth, as seen in Figure 2e and f, resembling what is typically observed for high quality InGaN epilayers grown by plasma-assisted MBE under nearly metal-rich conditions. ²⁹ The most interesting feature of this growth regime is the emergence of a very narrow, fin-shaped InGaN nanoridge on top of the triangular InGaN nanoprism, which is the focus of our results.

PL emission spectra of samples A-C were measured at room-temperature and are given in Figure 2g. A 405 nm laser

source was used as the excitation source with a $100\times$ objective and a beam $\sim 1~\mu m$ in diameter. For samples A and B, the peak wavelengths of InGaN nanostructures were 468 and 452 nm, respectively. For sample C, the PL emission of InGaN nanoridge/nanoprism showed a peak at 545 nm with intensity nearly 2 orders of magnitude stronger than that of samples A and B, as shown in logarithmic scale in Figure S2. In addition, a weak emission of ~ 450 nm was measured from sample C. These studies suggest that, under optimum growth conditions

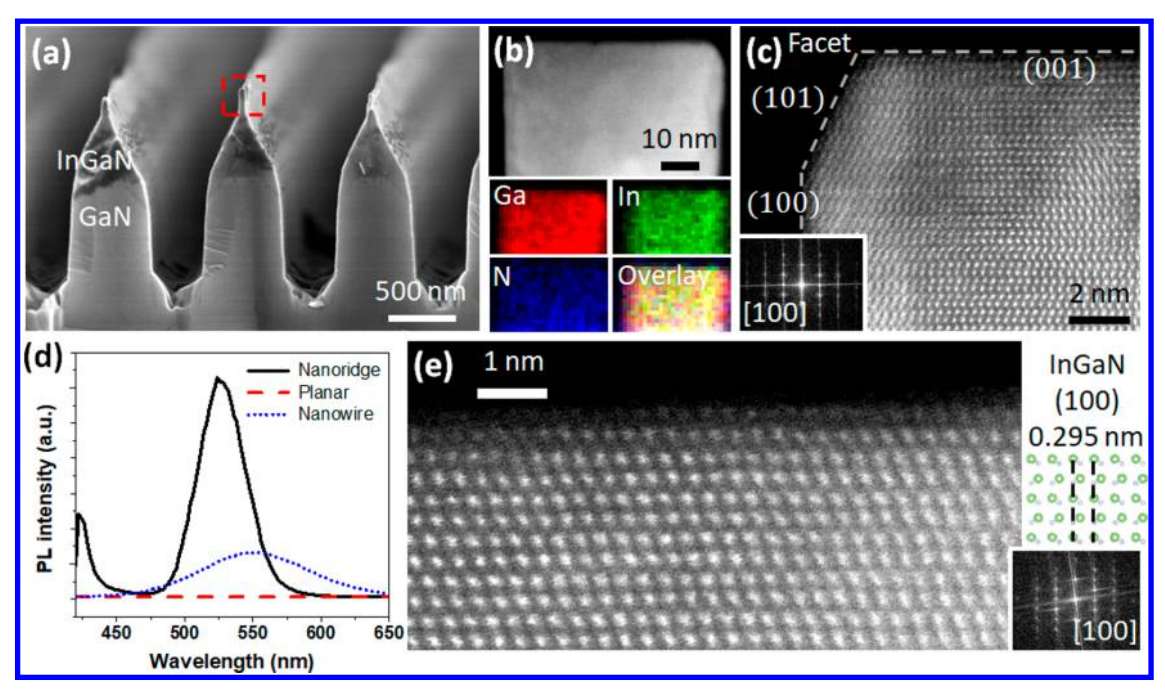


Figure 4. Single-crystal 1D InGaN nanoridge grown on GaN nanowall array (a) Side-view SEM (b) HAADF STEM image on cross-sectional finshaped InGaN nanoridge from one of the InGaN nanoridge/GaN nanowall arrays in (a) and simultaneous STEM EDS spectroscopic mapping showing the grown InGaN tip primarily comprised of Ga (red), In (blue), and N (green). (c) High-resolution HAADF STEM on the sharply faceted InGaN nanoridge in (c) indicating highly single crystalline. (d) Room temperature micro-PL of InGaN nanoridge (black solid line), planar (red dashed line), and nanowire (blue short dotted line) measured with 405 nm laser source. Peak wavelength positions for 6 h InGaN nanoridge and InGaN nanowire samples are 524 and 546 nm, respectively. Full-width at half-maximum (fwhm) values for 6 h InGaN nanoridge and InGaN nanowire samples are 40 and 101 nm, respectively. (e) Atomic resolution HAADF STEM on the termination of the InGaN tip in (c) indicating the lattice constant that is consistent with InGaN.

(nearly metal-rich epitaxy conditions), the optical quality can be significantly enhanced for InGaN nanoridge/nanoprism structures. Furthermore, the presence of two emission peaks suggests nonuniform indium distribution. We attribute the strong PL intensity to the highly crystalline quality of the InGaN nanoridge grown on top of the nanoprism. Such nanoridge structure allows effective strain relaxation and therefore high crystalline material. The strong PL intensity of sample C may originate from favorable growth of high-quality InGaN material under slightly metal-rich conditions, which is analogous to conventional epitaxial film growth.²⁹ The redshift of the wavelength on sample C compared to samples A and B may be attributed to effective strain relaxation and reduced density of defects by improved wetting, which may promote incorporation of In with decreased nonradiative recombination sites.30

To further study the formation of InGaN nanoridge structures, we observed the evolution of InGaN structure grown on top of the single GaN nanowall segment using the growth conditions from sample C. Illustrated in Figure 3a-d are cross-sectional SEM images of the GaN nanowall template and InGaN nanostructure after 2, 4, and 6 h of growth, respectively. InGaN grows on top of the c-plane GaN nanowall in the form of a prismatic shape for up to 4 h, as seen in Figure 3a-c. This InGaN forms a nanoprism structure that is bound by r-planes. In crystal growth, the slowest growing facet will eventually determine the crystal plane.³¹ From observation, growth in the [0001] direction is faster than that in the $[10\overline{1}2]$ or $[10\overline{1}1]$ directions. Therefore, the (0001) facet will diminish, and the r-plane will dominate, resulting in pyramidal shape as growth proceeds.³² The angle between inclined side planes and the (0001) plane was 63° (Figure S3), which indicates that the

r-plane of InGaN nanoprism has a $(10\overline{1}1)$ facet. ^{31,32} The formation of a semipolar $(10\overline{1}1)$ r-plane facet in the nanoprism is consistent with the hexagonal pyramid formation in selfassembled growth (SAG) of wurtzite GaN nanowires. 32,33 The only difference is that SAG nanowires have six r-plane facets of equal size on top of perfect hexagonal pyramid, whereas our structure shows elongated prismatic shape along the $[11\overline{2}0]$ adirection. Growth interface of SAG nanowire and nanoprism are represented in Figure S4. After 4 h of growth, the structure evolves into a fin-shaped nanoridge on top of the nanoprism, which starts to elongate proportionally to the growth duration. This fin-shaped nanoridge structure has growth along the [0001] direction with their sidewalls being m-planes $(10\overline{10})$ and (1010) planes. This narrow fin-shaped InGaN nanoridge has not been observed in any other work to our knowledge. Figure 3e shows the magnified cross-sectional SEM image of a nanoridge segment on top of the InGaN nanoprism.

As shown in Figure 3f, the growth rate along the *c*-axis decreases from an average growth rate of 140 nm/h in the first 2 h of growth to 109 nm/h from the second to fourth hour of growth. We attribute this to the reduced probability of Ga and In adatoms reaching the top of the nanoprism. When the narrow fin-shaped InGaN nanoridge starts to form, the chance of Ga and In adatoms migrating to the tip lowers even farther, reducing the growth rate to 91 nm/h from the fourth to sixth hour of growth. This growth rate reduction is consistent with the previous studies of reduced axial growth rate of self-assembled GaN nanowires over time. He SAG nanowires, Ga adatoms supplied by diffusion on a Mo mask need to diffuse to the top of GaN nanocolumns to contribute to the axial growth. Similarly, in InGaN nanoridge, both Ga and In adatoms will need to diffuse to the tip of the nanoridge, which

will be more challenging as the growth along the axial direction proceeds.

In this study, we did not observe any significant growth (>20 nm/h) along the lateral direction on the sidewall of the GaN nanowall. The epitaxy proceeds in a way to reveal the plane that has the lowest surface energy. The surface energy of the m-plane is lower than that of other nonpolar crystal planes. Therefore, the m-plane, which is the slowest growing plane, will be what forms the nanowall sidewall, which is supported by our observations. This is analogous to the previously reported SAG nanowire going through morphological evolution toward a thermodynamically stable hexagonal shape with m-planes. ³³

Room-temperature micro-PL spectra of the InGaN nanostructure grown on GaN nanowall with various growth durations are shown in Figure S5. As the growth duration increased from 2 to 6 h, we observed an increase in the intensity of the peak emission above 500 nm. After 4 h, the narrow fin-shaped InGaN nanoridge structure emerged, and we measured extremely strong PL emission. The indium incorporation is further derived using the equation

$$E_{\text{In}_x\text{Ga}_{1-x}\text{N}} = xE_{\text{InN}} + (1-x)E_{GaN} - bx(1-x)$$

The InGaN nanostructure sample is shown to have $x \sim 0.3$, where we used b = 1.10 eV as the average bowing parameter.³ To further verify that the emission is coming from the narrow fin-shaped InGaN nanoridge structure, we compared with the signal from InGaN grown on a planar region near the nanoridge/nanoprism. Figure S6 shows a schematic of the laser beam spot position at which PL was measured for the InGaN planar region and nanoridge/nanoprism region. The PL from the planar region showed negligible intensity compared to that from the nanoridge/nanoprism region, suggesting that the signal is coming from the InGaN grown on the GaN nanowall array template. This leaves two possible cases: the signal is from the nanoridges or from the InGaN between the nanowalls. If the emission originates from the InGaN between the GaN nanowall segments, these samples would show a strong PL emission at ~524-560 nm regardless of the GaN nanowall width. On the other hand, if the emission is coming from the InGaN nanoridge/nanoprism, the emission will depend on the presence of the nanoridge/nanoprism because InGaN growth atop wider GaN nanowalls does not have the InGaN nanoridge. To confirm that the signal is not from the InGaN grown between GaN nanowall segments, we prepared GaN nanowall templated samples with widths of 500, 800, and 1200 nm but the same spacing between walls. InGaN was grown on the GaN nanowall templates for 4 h. For this growth time, we only expect to see an InGaN nanoridge on the 500 nm width sample. From Figure S7a and b, emission from samples with wall widths of 800 and 1200 nm shows a negligible peak at ~524-560 nm, indicating that the strong emission at 524-560 nm is coming from the InGaN nanoridge. These studies also indicate that the weak emission measured below 500 nm is likely from the InGaN nanoprism and/or InGaN layer grown on the bottom between the GaN nanowall spacings.

PL emission was also measured for InGaN nanowire arrays with peak emission at 546 nm, as shown in Figure 4d (see Figure S8 for nanowire sample details). We found that the InGaN nanoridge structures exhibit intensity nearly 4-times higher than that of spontaneously formed InGaN nanowires despite the relatively small surface area of nanoridge structures.

Moreover, the emission of the nanoridge sample is sharper with a full-width-at-half-maximum (fwhm) value of 40 nm when compared to the fwhm value of 101 nm for the nanowire sample.

InGaN crystals were grown with hierarchical order that spans the nano- to atomic scale through lithographic templating (Figure 4a-c). Cross-sectional electron microscopy shows the periodic GaN nanowalls (width, ~500 nm; height, \sim 1 um; spacing, \sim 400–500 nm) that template-confined InGaN growth (Figure 4a). The single crystallinity of the InGaN nanoridge (~50 nm width) that forms along the top of each InGaN nanoprism is reflected in the sharply faceted termination of (100) sidewalls and (001) top (Figure. 4c) of the 6 h grown sample. In confined geometry heteroepitaxy, increased In incorporation can occur due to the onset of strainrelaxed growth.³⁹ In the 4 h sample, the InGaN nanoridge was formed with smaller width and height than that of the 6 h sample. In addition, this nanoridge was highly crystalline but lacked the sharp facets and contained a partially amorphous surface termination (Figure S9), suggesting that with further growth the nanoridge may crystallize and facet. An energydispersive X-ray (EDS) map shows a well-defined InGaN nanoridge after 6 h of growth homogeneously composed of Ga, In, and N without phase segregation (Figure 4b, Figure S10). This homogeneous distribution of Ga and In elements in our InGaN nanoridge is superior to that of InGaN growth on a randomly oriented c-axis GaN nanowall, where Rodriguez et al. observed strong fluctuation of the In composition in their structure.²¹ Energy-dispersive X-ray (EDX) spectra collected from four InGaN nanoridge regions estimates In occupies 27 ± 5% of Ga sites (i.e., $x = 0.27 \pm 0.05$). Pure GaN regions confirmed EDX quantification of Ga concentration to within ~10%. This In occupancy result is consistent with the PL result estimated to having $x \sim 0.3$ for InGaN. Atomicresolution dark-field scanning transmission electron microscopy (STEM) shows lattice spacings of 2.85 and 2.95 Å (Figure 4e, Figure S9) and confirms an In-rich InGaN crystal (GaN and InN spacings are 2.75 and 3.06 Å, respectively). This corresponds to the (100) lattice plane of InGaN with an orientation that indicates preferred growth along the [0001] caxis direction. Lastly, the highly ordered 1D InGaN provides strong PL emission (Figure 4d).

In summary, we have investigated the epitaxy and structural and optical characterization of InGaN nanoridge structures grown on a Ga-polarity GaN nanowall template. It is observed that a nearly defect-free fin-shaped InGaN nanoridge emerges from the c-axis InGaN bulk nanoprism structure, which can exhibit superior structural and optical properties. Under optimized growth conditions, PL emission from this InGaN nanoridge structure exhibits much higher intensity than InGaN grown on a planar structure or spontaneously formed InGaN nanowire arrays. Detailed structural study of this growth regime over the growth time clearly shows the structural evolution of the bulk triangular InGaN nanoprism into a very narrow, fin-shaped InGaN nanoridge. Atomic-resolution HAADF STEM and simultaneous STEM EDS spectroscopic mapping also suggests that this InGaN nanoridge structure is single crystalline with homogeneous In distribution. We envision that our integration of top-down and bottom-up approaches to obtain single-crystalline InGaN nanoridges with high In content will emerge as a viable architecture for designing a broad range of III-nitride devices. Moreover, further reducing the dimensions to the nanometer range may

provide an extremely scaled quantum material platform for next-generation ultrahigh efficiency electronic, photonic, and solar energy devices and systems.

ASSOCIATED CONTENT

S Supporting Information

The Supporting Information is available free of charge on the ACS Publications website at DOI: 10.1021/acs.cgd.8b01211.

Methods for PL and electron microscopy, nanowire versus nanoridge comparison table, SEM image of GaN nanowall array, detailed linear and logarithmic PL comparison curve, SEM image of nanoridge cross-section, nanoridge growth contour, schematic depicting PL beam spot position, SEM image of nanowire, and STEM-EDS map of nanoridge (PDF)

AUTHOR INFORMATION

Corresponding Author

*E-mail: ztmi@umich.edu; Phone: 734 764-3963.

ORCID

Yong-Bum Park: 0000-0001-5317-7975 Zetian Mi: 0000-0001-9494-7390

Notes

The authors declare no competing financial interest.

ACKNOWLEDGMENTS

The authors acknowledge support from the National Science Foundation (NSF) (ECCS-1709207) and Michigan Center for Materials Characterization (MC2) and technical support from Dr. Kai Sun. R.H. acknowledges support from DOE Office of Science (DE-SC0011385).

REFERENCES

- (1) Laubsch, A.; Sabathil, M.; Baur, J.; Peter, M.; Hahn, B. High-Power and High-Efficiency InGaN-Based Light Emitters. *IEEE Trans. Electron Devices* **2010**, *57*, 79–87.
- (2) Okamoto, K.; Ohta, H.; Nakagawa, D.; Sonobe, M.; Ichihara, J.; Takasu, H. Dislocation-Free m -Plane InGaN/GaN Light-Emitting Diodes on m -Plane GaN Single Crystals. *Jpn. J. Appl. Phys.* **2006**, 45, L1197—L1199.
- (3) Jani, O.; Ferguson, I.; Honsberg, C.; Kurtz, S. Design and characterization of GaN/InGaN solar cells. *Appl. Phys. Lett.* **2007**, *91*, 132117.
- (4) Dahal, R.; Pantha, B.; Li, J.; Lin, J. Y.; Jiang, H. X. InGaN/GaN multiple quantum well solar cells with long operating wavelengths. *Appl. Phys. Lett.* **2009**, *94*, 063505.
- (5) Fan, S.; Shih, I.; Mi, Z. A Monolithically Integrated InGaN Nanowire/Si Tandem Photoanode Approaching the Ideal Bandgap Configuration of 1.75/1.13 eV. Adv. Energy Mater. 2017, 7, 1600952.
- (6) Fan, S.; Woo, S. Y.; Vanka, S.; Botton, G. A.; Mi, Z. An In0.5Ga0.5N nanowire photoanode for harvesting deep visible light photons. *APL Mater.* **2016**, *4*, 076106.
- (7) Kibria, M. G.; Mi, Z. Artificial photosynthesis using metal/nonmetal-nitride semiconductors: current status, prospects, and challenges. *J. Mater. Chem. A* **2016**, *4*, 2801–2820.
- (8) Okamoto, N.; Hoshino, K.; Hara, N.; Takikawa, M.; Arakawa, Y. MOCVD-grown InGaN-channel HEMT structures with electron mobility of over. *J. Cryst. Growth* **2004**, *272*, *278*–284.
- (9) Laboutin, O.; Cao, Y.; Johnson, W.; Wang, R.; Li, G.; Jena, D.; Xing, H. InGaN channel high electron mobility transistor structures grown by metal organic chemical vapor deposition. *Appl. Phys. Lett.* **2012**, *100*, 121909.
- (10) Wang, R.; Li, G.; Karbasian, G.; Guo, J.; Faria, F.; Hu, Z.; Yue, Y.; Verma, J.; Laboutin, O.; Cao, Y.; Johnson, W.; Snider, G.; Fay, P.;

Jena, D.; Xing, H. InGaN Channel High-Electron-Mobility Transistors with InAlGaN Barrier and fT/fmax of 260/220 GHz. *Appl. Phys. Express* **2013**, *6*, 016503.

- (11) Van de Walle, C. G.; Neugebauer, J. Small valence-band offsets at GaN/InGaN heterojunctions. *Appl. Phys. Lett.* **1997**, *70*, 2577–2579.
- (12) Singh, R.; Doppalapudi, D.; Moustakas, T. D.; Romano, L. T. Phase separation in InGaN thick films and formation of InGaN/GaN double heterostructures in the entire alloy composition. *Appl. Phys. Lett.* **1997**, *70*, 1089–1091.
- (13) Hori, M.; Kano, K.; Yamaguchi, T.; Saito, Y.; Araki, T.; Nanishi, Y.; Teraguchi, N.; Suzuki, A. Optical Properties of InxGa1—xN with Entire Alloy Composition on InN Buffer Layer Grown by RF-MBE. *Phys. Status Solidi B* **2002**, 234, 750–754.
- (14) Guo, W.; Zhang, M.; Banerjee, A.; Bhattacharya, P. Catalyst-free InGaN/GaN nanowire light emitting diodes grown on (001) silicon by molecular beam epitaxy. *Nano Lett.* **2010**, *10*, 3355–3359.
- (15) Armitage, R.; Tsubaki, K. Multicolour luminescence from InGaN quantum wells grown over GaN nanowire arrays by molecular-beam epitaxy. *Nanotechnology* **2010**, *21*, 195202.
- (16) Woo, S. Y.; Bugnet, M.; Nguyen, H. P.; Mi, Z.; Botton, G. A. Atomic Ordering in InGaN Alloys within Nanowire Heterostructures. *Nano Lett.* **2015**, *15*, 6413–6418.
- (17) Wang, R.; Nguyen, H. P.; Connie, A. T.; Lee, J.; Shih, I.; Mi, Z. Color-tunable, phosphor-free InGaN nanowire light-emitting diode arrays monolithically integrated on silicon. *Opt. Express* **2014**, *22*, A1768–A1775.
- (18) Hazari, A.; Aiello, A.; Ng, T.-K.; Ooi, B. S.; Bhattacharya, P. III-nitride disk-in-nanowire $1.2\,\mu\mathrm{m}$ monolithic diode laser on (001)-silicon. *Appl. Phys. Lett.* **2015**, *107*, 191107.
- (19) Tamura, Y.; Hane, K. Optical characteristics of multiple layered InGaN quantum wells on GaN nanowalls grown on Si (111) substrate. *Mater. Res. Bull.* **2016**, 83, 563–567.
- (20) Zhong, A.; Hane, K. Characterization of GaN Nanowall Network and Optical Property of InGaN/GaN Quantum Wells by Molecular Beam Epitaxy. *Jpn. J. Appl. Phys.* **2013**, *52*, 08JE13.
- (21) Soto Rodriguez, P. E. D.; Kumar, P.; Gómez, V. J.; Alvi, N. H.; Mánuel, J. M.; Morales, F. M.; Jiménez, J. J.; García, R.; Calleja, E.; Nötzel, R. Spontaneous formation of InGaN nanowall network directly on Si. *Appl. Phys. Lett.* **2013**, *102*, 173105.
- (22) Goh, W. H.; Patriarche, G.; Bonanno, P. L.; Gautier, S.; Moudakir, T.; Abid, M.; Orsal, G.; Sirenko, A. A.; Cai, Z. H.; Martinez, A.; Ramdane, A.; Le Gratiet, L.; Troadec, D.; Soltani, A.; Ougazzaden, A. Structural and optical properties of nanodots, nanowires, and multi-quantum wells of III-nitride grown by MOVPE nano-selective area growth. *J. Cryst. Growth* **2011**, 315, 160–163.
- (23) Liu, X.; Zhao, S.; Le, B. H.; Mi, Z. Molecular beam epitaxial growth and characterization of AlN nanowall deep UV light emitting diodes. *Appl. Phys. Lett.* **2017**, *111*, 101103.
- (24) Bayerl, D.; Kioupakis, E. Visible-wavelength polarized-light emission with small-diameter InN nanowires. *Nano Lett.* **2014**, *14*, 3709–3714.
- (25) Chouksey, S.; Sankaranarayanan, S.; Pendem, V.; Saha, P. K.; Ganguly, S.; Saha, D. Strong Size Dependency on the Carrier and Photon Dynamics in InGaN/GaN Single Nanowalls Determined Using Photoluminescence and Ultrafast Transient Absorption Spectroscopy. *Nano Lett.* **2017**, *17*, 4596–4603.
- (26) Stocker, D. A.; Schubert, E. F.; Redwing, J. M. Crystallographic wet chemical etching of GaN. *Appl. Phys. Lett.* **1998**, *73*, 2654–2656.
- (27) Itoh, M.; Kinoshita, T.; Koike, C.; Takeuchi, M.; Kawasaki, K.; Aoyagi, Y. Straight and Smooth Etching of GaN (1100) Plane by Combination of Reactive Ion Etching and KOH Wet Etching Techniques. *Jpn. J. Appl. Phys.* **2006**, *45*, 3988.
- (28) Koblmüller, G.; Gallinat, C. S.; Speck, J. S. Surface kinetics and thermal instability of N-face InN grown by plasma-assisted molecular beam epitaxy. *J. Appl. Phys.* **2007**, *101*, 083516.
- (29) Gačević, Ž.; Gómez, V. J.; Lepetit, N. G.; Soto Rodríguez, P. E. D.; Bengoechea, A.; Fernández-Garrido, S.; Nötzel, R.; Calleja, E. A

comprehensive diagram to grow (0001)InGaN alloys by molecular beam epitaxy. *J. Cryst. Growth* **2013**, *364*, 123–127.

- (30) Komaki, H.; Katayama, R.; Onabe, K.; Ozeki, M.; Ikari, T. Nitrogen supply rate dependence of InGaN growth properties, by RF-MBE. J. Cryst. Growth 2007, 305, 12–18.
- (31) Jindal, V.; Shahedipour-Sandvik, F. Theoretical prediction of GaN nanostructure equilibrium and nonequilibrium shapes. *J. Appl. Phys.* **2009**, *106*, 083115.
- (32) Lundskog, A.; Forsberg, U.; Holtz, P. O.; Janzén, E. Morphology Control of Hot-Wall MOCVD Selective Area Grown Hexagonal GaN Pyramids. *Cryst. Growth Des.* **2012**, *12*, 5491–5496.
- (33) Gacevic, Z.; Gomez Sanchez, D.; Calleja, E. Formation mechanisms of GaN nanowires grown by selective area growth homoepitaxy. *Nano Lett.* **2015**, *15*, 1117–1121.
- (34) Urban, A.; Malindretos, J.; Klein-Wiele, J. H.; Simon, P.; Rizzi, A. Ga-polar GaN nanocolumn arrays with semipolar faceted tips. *New J. Phys.* **2014**, *16*, 019501.
- (35) Brubaker, M. D.; Duff, S. M.; Harvey, T. E.; Blanchard, P. T.; Roshko, A.; Sanders, A. W.; Sanford, N. A.; Bertness, K. A. Polarity-Controlled GaN/AlN Nucleation Layers for Selective-Area Growth of GaN Nanowire Arrays on Si(111) Substrates by Molecular Beam Epitaxy. Cryst. Growth Des. 2016, 16, 596–604.
- (36) Northrup, J. E.; Neugebauer, J. Theory of GaN (10–10) and (11–20) surfaces. *Phys. Rev. B: Condens. Matter Mater. Phys.* **1996**, 53, No. R10477(R).
- (37) Dreyer, C. E.; Janotti, A.; Van de Walle, C. G. Absolute surface energies of polar and nonpolar planes of GaN. *Phys. Rev. B: Condens. Matter Mater. Phys.* **2014**, *89*, No. 081305(R).
- (38) Moses, P. G.; Van de Walle, C. G. Band bowing and band alignment in InGaN alloys. Appl. Phys. Lett. 2010, 96, 021908.
- (39) Kuykendall, T.; Ulrich, P.; Aloni, S.; Yang, P. Complete composition tunability of InGaN nanowires using a combinatorial approach. *Nat. Mater.* **2007**, *6*, 951–956.